Numerical study of macroscopic pedestrian flow models

Monika Twarogowska, Paola Goatin, Régis Duvigneau

Numerical study of macroscopic pedestrian flow models

M. Twarogowska , P. Goatin , R. Duvigneau

RESEARCH REPORT

N° 8340

July 2013

Project-Teams Opale

ISSN 0249-6399 ISRN INRIA/RR--8340--FR+ENG

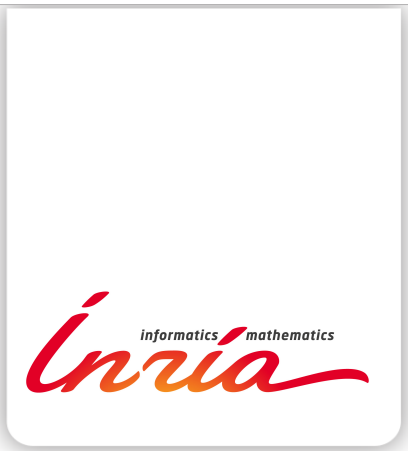

Numerical study of macroscopic pedestrian flow models

M. Twarogowska *, P. Goatin *, R. Duvigneau *

Project-Teams Opale

Research Report n° 8340 — July 2013 — 32 pages

Abstract: We analyze numerically macroscopic models of crowd dynamics: classical Hughes model and the second order model being an extension to pedestrian motion of the Payne-Whitham vehicular traffic model. The desired direction of motion is determined by solving an eikonal equation with density dependent running cost function standing for minimization of the travel time and avoidance of congested areas. We apply a mixed finite volume-element method to solve the problems and present error analysis in case of the eikonal solver, gradient computation and the second order model yielding a first order convergence. We show that Hughes' model is incapable of reproducing complex crowd dynamics such as stop-and-go waves and clogging at bottlenecks. Finally, using the second order model, we study numerically the evacuation of pedestrians from a room through a narrow exit. In particular, we analyze the effect on the total evacuation time of the level of compression, the desired speed and the presence of obstacles.

Key-words: macroscopic models, crowd dynamics, evacuation, finite volume methods

Author's adresses: INRIA Sophia Antipolis - Méditerranée, OPALE Project-Team, 2004, route des Lucioles – BP 93, 06902 Sophia Antipolis Cedex, France, e-mail: monika.twarogowska@inria.fr, paola.goatin@inria.fr, regis.duvigneau@inria.fr

* INRIA Sophia Antipolis - Méditerranée, OPALE Project-Team,

RESEARCH CENTRE
SOPHIA ANTIPOLIS – MÉDITERRANÉE

2004 route des Lucioles - BP 93
06902 Sophia Antipolis Cedex

Analyse numérique des modèles macroscopiques de la dynamique de foule

Résumé : On analyse plusieurs modèles numériques pour la dynamique des foules : le modèle classique de Hughes et le modèle du second ordre, qui est une extension au mouvement de piétons du modèle de Payne-Whitham pour le trafic routier. La direction du mouvement est obtenue par résolution d'une équation Eikonale avec une fonction de coût dépendant de la densité, de manière à minimiser le temps de déplacement et éviter les endroits congestionnés. On utilise une méthode mixte éléments / volumes finis pour résoudre le problème et on présente une analyse d'erreur pour la résolution de l'équation Eikonale, le calcul de gradient et le modèle du second ordre, aboutissant à une précision du premier ordre. On montre que le modèle de Hughes est incapable de reproduire la dynamique des foules complexes, comme les ondes de type "stop-and-go" et le phénomène de colmatage apparaissant aux goulots d'étranglement. Enfin, avec le modèle du second ordre, on étudie numériquement l'évacuation de piétons d'une salle avec une sortie étroite. An particulier, on analyse l'effet du niveau de compression, de la vitesse de déplacement et la présence d'obstacle sur le temps total d'évacuation.

Mots-clés : modèles macroscopiques, dynamique de la foule, évacuation, méthode volumes-finis

1 Introduction

Crowd dynamics has recently attracted the interests of a rapidly increasing number of scientists. Analytical and numerical analysis are effective tools to investigate, predict and simulate complex behaviour of pedestrians, and numerous engineering applications welcome the support of mathematical modelling. Growing population densities combined with easier transport lead to greater accumulation of people and increase risk of life threatening situations. Transport systems, sports events, holy sites or fire escapes are just few examples where uncontrolled behaviour of a crowd may end up in serious injuries and fatalities. In this field, pedestrian traffic management is aimed at designing walking facilities which follow optimal requirements regarding flow efficiency, pedestrians comfort and, above all, security and safety.

From a mathematical point of view, a description of human crowds is strongly non standard due to the intelligence and decisional abilities of pedestrians. Their behaviour depends on the physical form of individuals and on the purpose and conditions of their motion (see [41, 31, 19, 18, 21, 41]). Mathematical models describing crowd dynamics belong to two fundamentally distinct approaches: microscopic and macroscopic. Examples of microscopic models, in which pedestrians are treated as individual entities, are the social force model [22], cellular automata models [36, 8], AI-based models [13]. Macroscopic description treats the crowd as a continuum medium characterized by averaged quantities such as density and mean velocity. The first modelling attempt is due to Hughes [26] who defined the crowd as a "thinking fluid" and described the time evolution of its density using a scalar conservation law. Current macroscopic models use gas dynamics equations [1, 30], gradient flow methods [35], non linear conservation laws with non classical shocks [7] and time evolving measures [40].

We follow the macroscopic approach and analyze and compare two models. The first one, introduced by Hughes [26], consists of a mass conservation law supplemented with a phenomenological relation between the speed and the density of pedestrians. The second involves mass and momentum balance equations so is of the second order. It was proposed by Payne and Whitham [39, 49] to describe vehicular traffic and adopted to describe pedestrian motion by Jiang et al.[30]. In both models, the pedestrians' optimal path is computed using the eikonal equation as was proposed by Hughes [26].

In order to simulate realistic behaviour we consider two dimensional, continuous walking domains with impenetrable walls and exits as pedestrians' destination. To our knowledge the only available results using the Hughes' model concern simulations of flow of pedestrians on a large platform with an obstacle in its interior [25, 29]. In the case of the second order model Jiang et al. [30] considered the same simulation and showed numerically the formation of stop-and-go waves. However, none of the above works analyzed evacuation situations. This problem is an important safety issue because of arching and clogging appearing in front of the exit, which can interrupt the outflow and result in crushing of people under the pressure or the crowd. Experimental studies are rare due to the difficulties in reproducing realistic panic behaviour [32, 45, 23], while numerical simulations are available mainly in the microscopic framework [17, 20, 15].

The first aim of this paper is to provide a more detailed insight into the properties of the macroscopic models of pedestrian motion. In particular, we compare Hughes' model and the second order model analyzing the formation of stop-and-go waves and flows through bottlenecks. Our simulations suggest that Hughes' model is incapable of reproducing neither such waves nor clogging at a narrow exit. It appears to be also insensitive to the presence of obstacles placed in the interior of the walking domain, which can be crucial in the study of evacuation. This is why in the second part we restrict ourselves only to the second order model. At first we analyze the dependence of the solutions on different parameters of the model. More precisely, we consider

the effect on the evacuation of the strength of the interpersonal repealing forces and the desired speed of pedestrians. Both of these parameters may indicate the nervousness and the level of panic of pedestrians.

Then we study the evacuation from a room through a narrow exit following the idea of Hughes [27] who suggested that suitably placed obstacles can increase the flow through an exit. To our knowledge, so far this problem has been studied only numerically using the social force model [18, 10, 12]. We consider the second order model and try to improve the outflow of pedestrians through a door using obstacles placed in front of the exit. Motivated by the numerical simulations in which clogging appears when a large group of pedestrians reach the exit simultaneously, we give an example of five circular columns arranged in the shape of a triangle opened towards the exit. We show that this system of obstacles effectively creates an area with lower density in front of the door and prevents from clogging.

2 Macroscopic model of pedestrian flow

2.1 Equations

We consider a two dimensional connected domain $\Omega \subset \mathbb{R}^2$ corresponding to some walking facility. It is equipped with an exit which models the destination of the crowd motion and can contain obstacles. The boundary of the domain Ω is composed of the outflow boundary Γ_o and the wall Γ_w, which, as obstacles, is impenetrable for the pedestrians. In this setting we consider a macroscopic model introduced by Payne-Whitham for vehicular traffic flow in [39, 49] and by Jiang et al. in [30] to describe crowd dynamics. The model derives from fluid dynamics and consists of mass and momentum balance equations with source term. Denoting by ρ the density of pedestrians and by $\vec{v}$ their mean velocity the model reads

$$\begin{cases} \rho_t + \operatorname{div}(\rho\vec{v}) = 0, \\ (\rho\vec{v})_t + \operatorname{div}(\rho\vec{v}\otimes\vec{v}) = \vec{\mathcal{A}}, \end{cases} \tag{1a}$$

where $\vec{\mathcal{A}}$ describes the average acceleration caused by internal driving forces and motivations of pedestrians. More precisely, it consists of a relaxation term towards a desired velocity and the internal pressure preventing from overcrowding

$$\vec{\mathcal{A}} = \frac{1}{\tau}\left(\rho V(\rho)\vec{\mu} - \rho\vec{v}\right) - \nabla P(\rho). \tag{1b}$$

The unit vector $\vec{\mu} = \vec{\mu}(\rho(x,t))$ describes the preferred direction pointing the objective of the movement of pedestrians and is going to be defined in the next section. The function $V(\rho)$ characterizes how the speed of pedestrians changes with density. Various speed-density relations are available in the literature, see [6]. For our simulations we choose the exponential dependence

$$V(\rho) = v_{\max} e^{-\alpha\left(\frac{\rho}{\rho_{\max}}\right)^2}, \tag{2}$$

where $v_{\max}$ is a free flow speed, $\rho_{\max}$ is a congestion density at which the motion is hardly possible and α is a positive constant. The parameter τ in (1b) is a relaxation time describing how fast pedestrians correct their current velocity to the desired one. The second term in (1b) is a repulsive force modeling the volume filling effect and is given by the power law for isentropic gases

$$P(\rho) = p_0\rho^\gamma, \qquad p_0 > 0, \gamma > 1. \tag{3}$$

Remark: *Model (1) is referred to as a second order model as it consists of mass and momentum balance equations completed with a phenomenological law describing the acceleration. A simpler system, which is a first order model, was introduced by Hughes [26, 27]. It is composed of a scalar conservation law*

$$\rho_t + div(\rho V(\rho)\vec{\mu}) = 0 \tag{4}$$

closed by a speed-density relation $V(\rho)$ given by (2).

2.2 Desired velocity

The model (1), (4) have to be completed by defining the vector field $\vec{\mu}$. Following the works of Hughes, we assume that the pedestrians movement is opposite to the gradient of a scalar potential ϕ, that is

$$\vec{\mu} = -\frac{\nabla\phi}{||\nabla\phi||}. \tag{5}$$

The potential ϕ corresponds to an instantaneous travel cost which pedestrians want to minimize and is determined by the eikonal equation

$$\begin{cases} |\nabla\phi| = c(\rho) & \text{in} \quad \Omega \\ \phi = 0 & \text{on} \quad \Gamma_o \end{cases}, \tag{6}$$

where $c(\rho)$ is a density dependent cost function increasing with ρ. In the simplest case we could prescribe $c(\rho) = 1$, which gives the potential $\phi(x) = \text{dist}(x, \Gamma_o)$ in the case of convex domains. Pedestrians want to minimize the path towards their destination but temper the estimated travel time by avoiding high densities.The behaviour can be expressed by the "density driven" rearrangement of the equipotential curves of ϕ using the following cost function [26]

$$c(\rho) = \frac{1}{V(\rho)}. \tag{7}$$

Remark: *In the above model the definition of the preferred direction of motion corresponds to a situation in which pedestrians have a knowledge of the density distribution in the whole domain and on this basis estimate their travel time. This assumption in unrealistic in large, complicated domains where an overview of the whole area is impossible. Then it is reasonable that only the location of the destination point and the local density are known. This approach was introduced in [50] for the first order model by re-defining the direction vector $\vec{\mu}$. More precisely, the authors assumed that pedestrians seek to minimize their estimated travel cost based on memory of the exit location but temper this behaviour to avoid high densities only in their proximity. This hypothesis leads to*

$$\vec{\mu} = \frac{-\nabla\phi - \omega\nabla\left[V(\rho)^{-1} + g(\rho)\right]}{||-\nabla\phi - \omega\nabla\left[V(\rho)^{-1} + g(\rho)\right]||} \tag{8}$$

where the potential ϕ is given by (6) with $c(\rho) = 1/v_{\max}$, ω is a positive constant representing the psychological influence and $g(\rho) = g_0\left(\frac{\rho}{\rho_{\max}}\right)^2$ is a discomfort field due to the presence of other pedestrians.

3 Numerical scheme

Let us now present the numerical scheme on unstructured triangular mesh that we used to perform numerical simulations. The model of pedestrian flow couples equations of different

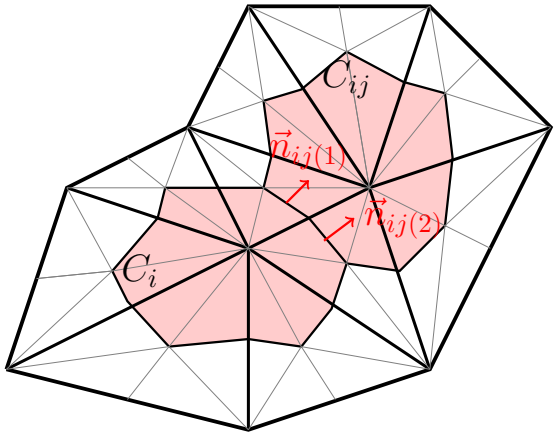

Figure 1: Dual cells of the unstructured triangular mesh

nature, i.e. a two dimensional non-linear system of conservations laws with sources, coupled with the eikonal equation through the source term. In this section we describe a finite volume scheme built on dual cells for system (1) and (4) and a finite element method based on the variational principle for problem (6). The numerical simulations are carried out using the multidisciplinary platform NUM3SIS developed at Inria Sophia Antipolis [28, 33].

3.1 Finite volume schemes

According to the framework of finite volume schemes, we decompose the domain Ω into N non overlapping, finite volume cells C_i, $i = 1, ..., N$, given by dual cells centered at vertices of the triangular mesh. For each cell C_i we consider a set of N_i neighbouring cells C_{ij}, $j = 1, ..., N_i$. By e_{ij} we denote the face between C_i and C_{ij}, $|e_{ij}|$ its length and $\vec{n}_{ij}$ is a unit vector pointing from the center of the cell C_i towards the center of the cell C_{ij}, see Figure 1.
The solution U on a cell C_i is approximated by the cell average of the solution at time $t > 0$, that is

$$U_i = \frac{1}{|C_i|} \int_{C_i} U(x,t)dx.$$

3.1.1 Space discretization of the second order model (1)

At first we are going to give details of a finite volume scheme for the model (1). Let us denote by $U = (\rho, \rho\vec{v})^T$ the unknowns vector, density and momentum. Then system (1) can be written in the following form

$$U_t + \mathrm{div}\vec{F}(U) = S(U), \tag{9a}$$

$$\vec{F}(U) = \begin{pmatrix} F^{\rho} \\ F^{\rho\vec{v}} \end{pmatrix} = \begin{pmatrix} \rho\vec{v} \\ \rho\vec{v} \otimes \vec{v} + P(\rho) \end{pmatrix}, \quad S(U) = \begin{pmatrix} 0 \\ \frac{1}{\tau}\left(\rho V(\rho)\vec{\mu} - \rho\vec{v}\right) \end{pmatrix}. \tag{9b}$$

A general semi-discrete finite volume scheme for (9) can be defined as

$$\frac{d}{dt}U_i = -\frac{1}{|C_i|}\sum_{j=1}^{N_i} |e_{ij}|\mathcal{F}(U_i, U_j, \vec{n}_{ij}) + S(U_i), \tag{10}$$

where $\mathcal{F}(U_i, U_j, \vec{n}_{ij})$ is a numerical flux computed in a one dimensional mode across the fan e_{ij} between cells C_i and C_j along the normal direction $\vec{n}_{ij}$. The spatial discretization of the source term $S(U_i)$ is treated by a pointwise approximation

$$S(U_i) = \begin{pmatrix} 0 \\ \frac{1}{\tau}\left(\rho_i V(\rho_i)\vec{\mu}_i - \rho_i \vec{v}_i\right) \end{pmatrix}. \tag{11}$$

HLL flux function

In order to obtain a numerical approximation using a finite volume scheme (10) we have to calculate numerical fluxes $\mathcal{F}(U_i, U_j, \vec{n}_{ij})$ between control cells C_i and C_{ij} along the direction $\vec{n}_{ij}$. Despite the fact that the model is two space dimensional, these fluxes are computed using a one-dimensional approximation. They are based on solving the Riemann problem at each facet in exact or approximate form.

The homogeneous part of the model (1) coincides with the isentropic gas dynamics system for which many solvers are available, (see [47]). However, the occurrence of vacuum may cause instabilities and not all of them preserve non negativity of the density. We use the first order HLL approximate Riemann solver [14]. It assumes that the solution consists of three constant states separated by two waves with speeds σ_L and σ_R corresponding respectively to the slowest and fastest signal speeds. It preserves non negativity of the density under certain conditions on the above numerical wave speeds [9].

Let us now present the HLL approximate Riemann solver applied to the normal component of the analytical flux that is to $\vec{F} \cdot \vec{n}$ where $\vec{F}$ is given by (9b). We consider two states U_L, U_R

$$U_K = (\rho_K, \rho_K u_K, \rho_K v_K)^T, \qquad K = L, R, \tag{12}$$

where $\vec{v} = [u, v]$, at any two control cells C_L (left), C_R (right). Moreover we denote the analytical flux and the pressure function calculated at these states by $\vec{F}_K = \vec{F}(U_K)$, $P_K = P(\rho_K)$ respectively. The normal component of the velocity is given by $v_K^n = \vec{v}_K \cdot \vec{n}$. The HLL numerical flux can be written in the following form

$$\mathcal{F}(U_L, U_R, \vec{n}) = \begin{cases} \vec{F}_L \cdot \vec{n} & \text{if} \quad \sigma_L > 0 \\ F^* & \text{if} \quad \sigma_L \le 0 \le \sigma_R \\ \vec{F}_R \cdot \vec{n} & \text{if} \quad \sigma_L \le \sigma_R < 0 \end{cases}, \tag{13a}$$

where

$$\vec{F}_K \cdot \vec{n} = F_K^n = \begin{cases} \rho_K v_K^n \\ \rho_K v_K^n u_K + P_K n_1 \\ \rho_K v_K^n v_K + P_K n_2 \end{cases}, \quad K = L, R, \tag{13b}$$

and the intermediate flux is given by

$$F^* = \begin{cases} \dfrac{\sigma_R \rho_L v_L^n - \sigma_L \rho_R v_R^n + \sigma_L \sigma_R (\rho_R - \rho_L)}{\sigma_R - \sigma_L} \\ \dfrac{\sigma_R(\rho_L v_L^n u_L + P_L n_1) - \sigma_L(\rho_R v_R^n u_R + P_R n_1) + \sigma_L \sigma_R(\rho_R u_R - \rho_L u_L)}{\sigma_R - \sigma_L} \\ \dfrac{\sigma_R(\rho_L v_L^n v_L + P_L n_2) - \sigma_L(\rho_R v_R^n v_R + P_R n_2) + \sigma_L \sigma_R(\rho_R v_R - \rho_L v_L)}{\sigma_R - \sigma_L} \end{cases}. \tag{13c}$$

The estimates of the wave speeds σ_L and σ_R have to assure that the density remains always non negative. Following [9], we use Roe's averages that is

$$\begin{aligned} \sigma_L &= \min(v_L^n - s_L, \bar{v}_{Roe} - \bar{s}), \\ \sigma_R &= \max(\bar{v}_{Roe} + \bar{s}, v_R^n + s_R), \end{aligned} \tag{14}$$

where

- $s_K = \sqrt{P'(\rho_K)}$ - sound speed,
- $\bar{v}_{Roe} = \dfrac{\sqrt{\rho_L}v_L^n + \sqrt{\rho_R}v_R^n}{\sqrt{\rho_L} + \sqrt{\rho_R}}$ - averaged Roe's velocity,
- $\bar{s} = \sqrt{(\gamma - 1)\left(\bar{H}_{Roe} - \dfrac{1}{2}\bar{v}_{Roe}^2\right)}$ - averaged sound speed,
- $\bar{H}_{Roe} = \dfrac{\sqrt{\rho_L}H_L + \sqrt{\rho_R}H_R}{\sqrt{\rho_L} + \sqrt{\rho_R}}$ - averaged Roe's enthalpy,
- $H_K = \dfrac{1}{2}\left(v_K^n\right)^2 + \dfrac{1}{\gamma - 1}P'(\rho_K)$ - enthalpy.

3.2 Space discretization of the first order model (4)

The numerical approximation at cell C_i of the solution to the first order model (4) ρ_i is obtained using the same general finite volume scheme (10) as for the second order system. For the numerical function we use the Lax-Friedrichs flux

$$\mathcal{F}\left(\rho_i, \rho_j, \vec{n}_{ij}\right) = \frac{1}{2}\left[G(\rho_i)\cdot\vec{n}_{ij} + G(\rho_j)\cdot\vec{n}_{ij} - \xi(\rho_j - \rho_i)\right], \tag{15a}$$

where $G(\rho) = \rho V(\rho)\vec{\mu}$ is the analytical flux of the model (4). The numerical viscosity coefficient ξ and the direction vector $\vec{\mu}$ depend on the density that is

$$\xi = \max_{l=i,j}\left|\frac{d}{d\rho}G(\rho_l)\right| = \max_{l=i,j}\left|\frac{d}{d\rho}\left(\rho_l V(\rho_l)\vec{\mu}_l(\rho)\right)\right| = \max_{l=i,j}\left|\frac{d}{d\rho}\left(\rho_l V(\rho_l)\right)\right|. \tag{15b}$$

The last equality is justified by the fact that $\vec{\mu}$ is a unit vector.

3.3 Fully discrete scheme

The difficulty in the time discretization of equation (10) lies in the non linear coupling of the models with the eikonal equation (6) in the flux for the first order model and in the source term for the second order one. This is why we apply explicit time integration method. Denoting the time step by Δt, the density at the time step t^{n+1} in the case of the first order model is obtained using the explicit Euler method

$$\rho_i^{n+1} = \rho_i^n - \frac{\Delta t}{|C_i|}\sum_{j=1}^{N_i}|e_{ij}|\mathcal{F}(\rho_i^n, \rho_j^n, \vec{n}_{ij}), \tag{16}$$

where the numerical flux function $\mathcal{F}$ depends explicitly on $\vec{\mu}^n$. The stability is achieved under the CFL condition $\Delta t \leq \alpha\dfrac{\min_{i=1,\ldots,N}\text{diameter}(C_i)}{\sigma_i}$. Using the speed-density relation (2) the maximal wave speed σ_i is given by

$$\begin{aligned}\sigma_i &= \max_{i=1,\ldots N}\left|\frac{d}{d\rho}F(\rho)\right| \\ &= \max_{i=1,\ldots N}\left|\left(v_{\max}e^{-\alpha\left(\frac{\rho_i}{\rho_{\max}}\right)^2} - 2\alpha v_{\max}\left(\frac{\rho_i}{\rho_{\max}}\right)^2 e^{-\alpha\left(\frac{\rho_i}{\rho_{\max}}\right)^2}\right)\right| = v_{\max}\end{aligned} \tag{17}$$

due to the same argument $|\vec{\mu}| = 1$ used for the computation of the coefficient ξ in the Lax-Friedrichs flux (15). The value of α is set to 0.9 in the following computations.

The second order model contains the source term in the momentum balance equation. We use the splitting technique between the transport and the source in the form

$$\begin{cases} U_i^* = U_i^n - \dfrac{\Delta t}{|C_i|} \displaystyle\sum_{j=1}^{N_i} |e_{ij}| \mathcal{F}(U_i^n, U_j^n, \vec{n}_{ij}), \\ U_i^{n+1} = U_i^* + \Delta t S(U_i^*). \end{cases} \tag{18}$$

The stability of the scheme is assured by the following CFL condition

$$\Delta t \leq 0.9 \frac{\min_{i=1,\ldots,N} \text{diameter}(C_i)}{\sigma_i}, \tag{19}$$

where $\sigma_i = \max\limits_{j=1,\ldots,N_i} (\vec{v}_i \cdot \vec{n}_{ij}) + \sqrt{P'(\rho_i)}$ is the maximal value of the characteristic wave speed of the homogeneous part of the system (1).

3.4 Eikonal equation and gradient

To obtain the solution at time step t^{n+1} we need to compute the direction vector $\vec{\mu}$ defined by (5). It means that we have to solve the eikonal equation (6) and compute the gradient of its solution. Equation (6) is a special case of the static Hamilton-Jacobi equation, for which many numerical methods have been developed such as level-set methods [38, 37], fast marching and fast sweeping methods [43, 48], semi-lagrangian scheme [11], finite volume or finite element schemes [24, 5]. We implement the Bornemann and Rasch algorithm [2] belonging to the last of the above approaches thus it is easier to implement on unstructured triangular meshes with respect to other methods. It is a linear, finite element discretization based on the solution to a simplified, localized Dirichlet problem solved by the variational principle.

Let Ω_i be a neighborhood of a node $x_i \in \Omega_h$ that is a local domain composed of triangles having the node x_i as its vertex (see Fig 2a). By $V(i)$, $\mathcal{V}_i$ we denote a set of global indices of vertices and points x in the direct neighborhood of a point $x_i \in \partial\Omega_i$ respectively, $V(i) = \{N(i,l), l \in \mathcal{V}(i)\}$. The local eikonal problem is given by

$$|\nabla\phi| = c(\rho_i) \quad \text{in} \quad \Omega_i, \qquad \phi(x) = \phi_h(x) \quad \text{on} \quad \partial\Omega_i. \tag{20}$$

The Hopf-Lax update function has the form

$$\phi(x_i) = \min_{y \in \partial\Omega_i} \left(\phi_h(y) + |x_i - y| c(\rho_i) \right), \tag{21}$$

where $|\cdot|$ denotes a norm of a vector. To evaluate the above formula let us consider only one of the triangles T_{ij} and call its vertices x_i, y_i, z_i (see Fig 2b). Then the update (21) becomes

$$\phi(x_i) = \min_{j \in \mathcal{V}(i)} \min_{y \in [y_i, z_i]} \left(\phi_h(y) + |x_i - y| c(\rho_i) \right) = \min_{j \in \mathcal{V}(i)} \left(\phi_j^* \right), \tag{22}$$

where $[y_i, z_i]$ is a closed edge of a triangle T_{ij} opposite to the vertex x_i. Defining $\Delta := \frac{\phi_h(z_i) - \phi_h(y_i)}{|z_i - y_i| c(\rho_i)}$ and using a geometric argument, (see [2] for details), the minimum value ϕ_j^* can be found explicitly

$$\phi_j^* = \begin{cases} \phi_h(y_i) + |y_i - x_i| c(\rho_i) & \text{if} \quad \cos(\alpha) < \Delta \\ \phi_h(y_i) + \xi |y_i - x_i| c(\rho_i) & \text{if} \quad -\cos(\beta) \leq \Delta \leq \cos(\alpha) \\ \phi_h(z_i) + |z_i - x_i| c(\rho_i) & \text{if} \quad \Delta < -\cos(\beta) \end{cases}, \tag{23}$$

where $\xi = \cos(\alpha)\Delta + \sqrt{(1-\cos^2(\alpha))(1-\Delta^2)}$,

$$\cos(\alpha) = \frac{(x_i - y_i)\cdot(y_i - z_i)}{|x_i - y_i||y_i - z_i|}, \qquad \cos(\beta) = \frac{(x_i - z_i)\cdot(y_i - z_i)}{|x_i - z_i||y_i - z_i|},$$

and $x \cdot y$ denoting the scalar product between vectors x, y.

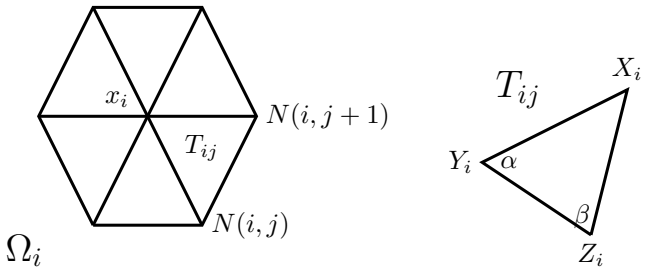

Figure 2: *On the left: The neighborhood Ω_i of a node $x_i \in \Omega$, that is, a collection of all triangles of the mesh that have x_i as a vertex. On the right: One of the triangles T_{ij} that have the node x_i as a vertex.*

Iterative update of the solution is initialized with $\phi_h^0 = 0$ on $\partial\Omega = \Gamma_{outflow}$ and $\phi_h^0 = \infty$ elsewhere. Iterations end if $||\phi_h^{n+1} - \phi_h^n||_{L^\infty} \leq$ tolerance where ϕ_h^{n+1} is obtained using the update formula (22), (23).

Having found the potential ϕ we calculate its gradient using the nodal P_1 Galerkin gradient method. It is related to cell C_i and is computed by averaging the gradients of all triangles having node i as a vertex. In two dimensions it has the form

$$\nabla\phi_i = \frac{1}{|C_i|}\sum_{T_{ij}\in C_i}\frac{|T_{ij}|}{3}\sum_{k\in T_{ij}}\phi_k \nabla P_k|_{T_{ij}}, \tag{24}$$

where T_{ij} are finite elements with the considered node i as a vertex, k counts for vertices of T_{ij} and $P_k|_{T_{ij}}$ is a P_1 basis function associated with vertex k.

3.5 Boundary conditions

We perform simulations on a two-dimensional domain $\Omega \subset \mathbb{R}^2$ with boundary $\partial\Omega = \Gamma_o \cup \Gamma_w$, see Fig 3. We set the outflow boundary Γ_o far from the exit of the room through which pedestrians go out so that the outflow rate doesn't influence the flow through the door. We assume that pedestrians cannot pass through walls, but can move along them that is we impose free-slip boundary conditions

$$\vec{v}\cdot\vec{n} = 0, \frac{\partial\rho}{\partial n} = 0 \qquad \text{at } \Gamma_w. \tag{25}$$

We now give details on the boundary conditions for the first and the second order models.

3.5.1 Second order model

There are two main methods to impose boundary conditions: week and strong. The strong boundary conditions approach can be used when the value of one conservative variable is exactly known at the boundary. The weak method consists of computing the fluxes with any numerical

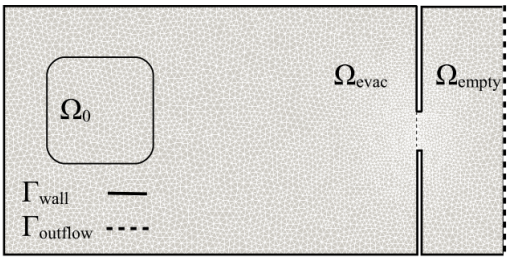

Figure 3: *Two dimensional domain* $\Omega_{evac} \cup \Omega_{empty} = \Omega \subset \mathbb{R}^2$ *with the boundary* $\partial\Omega = \Gamma_{wall} + \Gamma_{outflow}$. *Initially the density is positive only in the region* Ω_0

fluxes $\mathcal{F}(U_i, U_g, \vec{n})$ through boundary facets using an interior state U_i and a corresponding ghost state U_g and. In our study we follow the second approach and define the ghost state as a function of the interior one. In particular, we choose

$$\rho_g = \rho_i, \qquad \vec{v}_g = \vec{v}_i - 2(\vec{v}_i \cdot \vec{n})\vec{n} \tag{26}$$

at wall boundary Γ_w and

$$\rho_g = 0.1\rho_{\max}, \qquad \vec{v}_g = v_{\max}\vec{n} \tag{27}$$

for the outflow Γ_o.

Remark: *For the numerical flux function* $\mathcal{F}(U_i, U_g, \vec{n})$ *we use the HLL approximate Riemann solver (13). However, our numerical simulations show that the condition (25) is not satisfied at the wall boundary under the CFL condition* (19). *Sub iterations would be needed at each time step to converge to the correct solution. But due to the eikonal solver they become very expensive. To reduce the computational cost, after computing* U^* *in* (18) *we set to zero at wall boundary nodes the component of the velocity normal to the boundary. Adding the source term preserves the slip-wall boundary condition.*

Remark: (Mass conservation) *It is essential that there is no loss of the mass through the wall boundary during numerical simulation. The HLL solver (13) with the ghost state defined by (26) satisfies this condition when slip boundary condition (25) holds. In fact, let us consider four possible combinations of minimum and maximum wave speeds (14). Using* (26) *we get* $v_g^n = -v_i^n = 0$ *at the wall boundary, where the last equality is due to the previous Remark. Then we always have* $(\sigma_i, \sigma_g) = (-s_i, s_i)$, *where* $s_i = \sqrt{P'(\rho_i)}$. *Therefore the flux* $\mathcal{F}(U_i, U_g, \vec{n}) = F^*(U_i, U_g, \vec{n})$ *is given by (13c). There is no mass flow if the first component of* F^* *is zero which is true if* U_g *is defined by (26), because we have*

$$s_i\rho_i v_i^n - (-s_i)\rho_i(-v_i^n) + (-s_i)s_i(\rho_i - \rho_i) = 0 \tag{28}$$

3.5.2 First order model

The first order model consists only of mass conservation equation and the boundary conditions are imposed by defining directly the fluxes at boundary facets. More precisely, we set

$$\mathcal{F} = \begin{cases} 0 & \text{at} \quad \Gamma_w \\ \rho_{\max} V(\rho_{\max}) & \text{at} \quad \Gamma_o \end{cases} . \tag{29}$$

PARAMETER NAME	SYMBOL	VALUE	UNITS
desired speed	$v_{\max}$	$1-7$	$\frac{m}{s}$
relaxation time	τ	0.61	s
maximal density	$\rho_{\max}$	7	$\frac{\text{ped}}{m^2}$
pressure coefficient	p_0	$0.005-10$	$\frac{\text{ped}^{1-\gamma}\cdot m^{2+\gamma}}{s^2}$
adiabatic exponent	γ	$2-5$	-
density-speed coefficient	α	7.5	-

Table 1: *Parameters values used in the simulation*

3.6 Initial conditions

In our simulation we consider initial conditions of the form

$$\rho_0(x) = \begin{cases} \bar{\rho} & \text{in } \Omega_0 \\ 0 & \text{elsewhere} \end{cases}, \qquad \vec{v}_0(x) = 0, \tag{30}$$

where $\bar{\rho}$ is a positive constant and Ω_0 is an area inside the evacuation domain far from the exit, see Fig 3. This means that all pedestrians are placed inside the evacuation room and start to move at $t = 0$.

4 Numerical results

In this section we explore numerically the evacuation dynamics of pedestrians from a room through a narrow exit using model (1) and the numerical scheme presented in the previous section. This analysis is preceded by a numerical error analysis of the scheme and a comparison between the first (4) and the second (1) order model. We will see that the former is incapable of reproducing complex dynamics of crowd motion such as formation of stop-and-go waves and clogging at bottlenecks. Therefore, further study concerns only the second order model. We analyze the dependence of its solutions on some of the parameters of the system. In particular, we are interested in the effect of the strength of the internal repealing forces on evacuation. We analyze the behaviour for different values of the pressure coefficient p_0 and the adiabatic exponent γ. We also compare the evacuation for different desired speeds $v_{\max}$. Finally, we consider the evacuation from a room through a narrow exit. We analyze numerically a configuration of obstacles which creates a "waiting zone" in front of the exit. As a result, the outflow of pedestrians does not decrease due to clogging.

In numerical simulations we use the parameters listed in Table 4. Maximal velocity v_{max}, maximal density ρ_{max} and the response time τ are chosen from the available literature on experimental studies of pedestrian behaviour, (see [6, 46]). The values of some of the parameters of model (1), such as p_0, γ, α to authors' knowledge do not have a direct correspondence with the microscopic characteristics of pedestrian motion.

We introduce two functionals to analyze the results of simulations following discrete definition:

- Total mass of pedestrians inside the evacuation domain

$$M(t) = \int_\Omega \rho(x,t)dx, \qquad M^n = \sum_{i=1}^{N} \rho_i^n |C_i|. \tag{31}$$

- Total evacuation time

$$T_{\text{evac}} = \int_0^\infty M(t)dt, \qquad T_{\text{evac}} = \sum_{n=1}^{\infty} M^n \Delta t^n. \tag{32}$$

4.1 Order of convergence

In this section we analyze the accuracy of the numerical scheme presented in Section **??**. More precisely, we first estimate L^1 errors and convergence order of the method used to solve the eikonal equation and to compute its gradient. Then we perform the analysis for the fully discrete scheme for the second order model.

Let Ω_k be a mesh with N_k finite volume cells and δ_i be a surface area of the finite volume cell associated with the i-th vertex of the mesh Ω_k. We consider the L^1 error between the reference solution u_{ref} and the approximated one u_{h_k} in the form

$$E_k = \sum_{i=1}^{N_k} |u_{h_k}^i - u_{ref}^i| \delta_i. \tag{33}$$

We assume that

$$E_k^i = u_{h_k}^i - u_{ref}^i = Ch_k^p + h.o.t, \qquad C - constant. \tag{34}$$

The grid-spacing parameter h_k has the form $h_k = \sqrt{N_{ref}/N_k}$, where N_{ref} is the number of finite volume cells for the reference mesh (see [42]). When an explicit, analytical solution is available we replace N_{ref} with the area of the domain $|\Omega|$. We estimate the order of convergence p using the least square method applied to the logarithm of the equation (34) with neglected higher order terms.

4.1.1 Eikonal equation and gradient calculator

We are going to estimate the order of the algorithm presented in the previous section to solve the eikonal equation and to compute the gradient of its solution. In the following tests we use the running cost (7) with the speed-density relation given by (2) and $v_{\max} = 2\ m/s$ and $\rho_{\max} = 7\ ped/m^2$. Three cases are analyzed.

Test 1: We consider a domain $\Omega = [0,2] \times [0,0.2]$ with an outflow localized at $x = 0$ and density distribution $\rho(x) = x$. The solution to the eikonal equation (6) is found explicitly and is given by

$$\phi(x) = \int_0^x \frac{1}{V(\rho)} dx = -\frac{\rho_{\max}}{v_{\max}} \ln \left| 1 - \frac{x}{\rho_{\max}} \right|. \tag{35}$$

Its gradient equals

$$\vec{\nabla}\phi = \left[\frac{1}{V(\rho)}, 0 \right] = \left[\frac{1}{v_{\max}\left(1 - \frac{x}{\rho_{\max}}\right)}, 0 \right]. \tag{36}$$

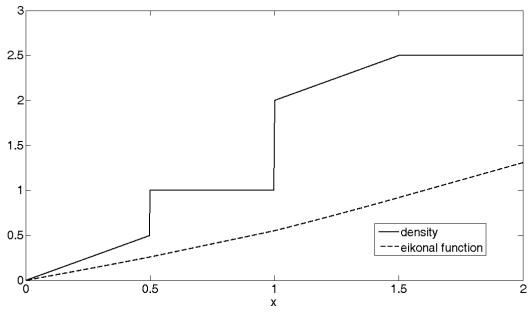

Figure 4: *Profile of the density distribution* $\Omega = [0, 2] \times [0, 0.2]$ *and the explicit solution to the eikonal equation.*

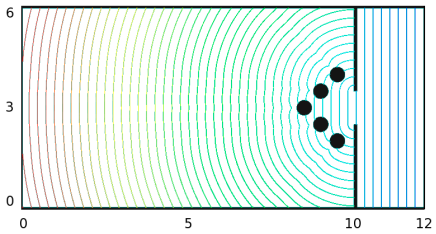

Figure 5: *A room* $10m \times 6m$ *with a* $1m$ *wide, symmetrically placed exit and columns with radius* $r = 0.23m$ *centered at* $(9.5, 2), (9, 2.5), (8.5, 3), (9, 3.5), (9.5, 4)$.

Test 2: We use the same domain as in Test 1 , see Fig 4,

$$\rho(x) = \begin{cases} x & if \quad x < 0.5 \\ 1 & if \quad 0.5 \leq x < 1 \\ x + 1 & if \quad 1 \leq x < 1.5 \\ 2.5 & if \quad x \geq 1.5 \end{cases} . \tag{37}$$

The solutions to the eikonal equation and the gradient can be found explicitly as in the Test 1.

Test 3: We analyze a domain $\Omega = [0, 10m] \times [0, 6m]$ with an exit of width $L = 1\ m$ centered at $(x, y) = (10, 3)$ and five columns of radius $r = 0.23\ m$ in its interior, see Fig 5. The density is set to zero everywhere and the reference solution is obtained on a very fine grid with $N = 136507$ finite volume cells.

In Fig 6 we present the dependence of the L^1 error on the mesh size that is on the number of finite volume cells N and the loglog plot of the dependence of the L^1 error on different grid-spacings h_k for the eikonal function and the components of its gradient. In Table 2 we present the corresponding estimates of the convergence order, obtained using the least square method. We observe that the values of the orders are close to one. In particular, gradient is computed with a higher order method and its computation does not decrease the order of the full scheme.

4.1.2 Numerical scheme for the second order model

Now we perform the same error analysis for the fully discrete scheme (18) for the second order model (1). We consider the same domain as in Test 2 in the previous section, but with initial

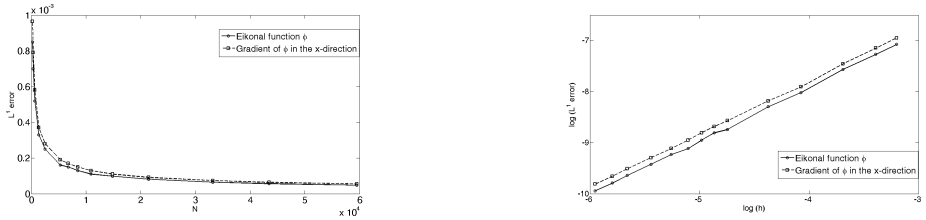

Test 1

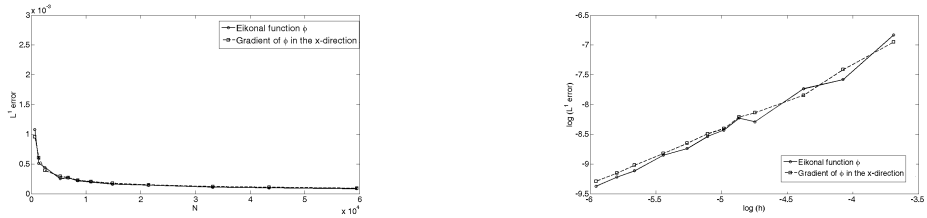

Test 2

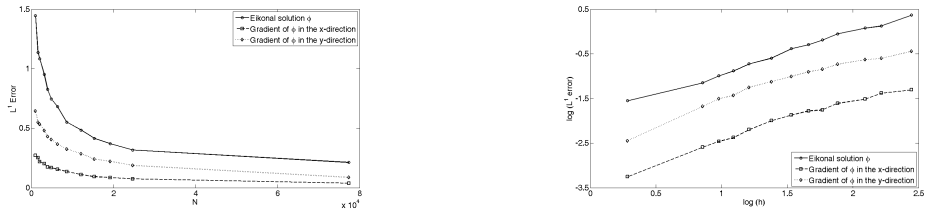

Test 3

Figure 6: *Dependence of the L^1 errors of the eikonal solution ϕ and its gradient in the x and y direction on the number of finite volume cells N (on the left) and the loglog plot of the errors with respect to the grid-spacing h (on the right).*

	Eikonal func.	Gradient-x	Gradient-y
Test 1	1.048	1.041	–
Test 2	1.063	1.012	–
Test 3	0.923	0.903	0.881

Table 2: *Estimates of the order of the eikonal solver presented in Section 3.4 and the method to compute a gradient (24).*

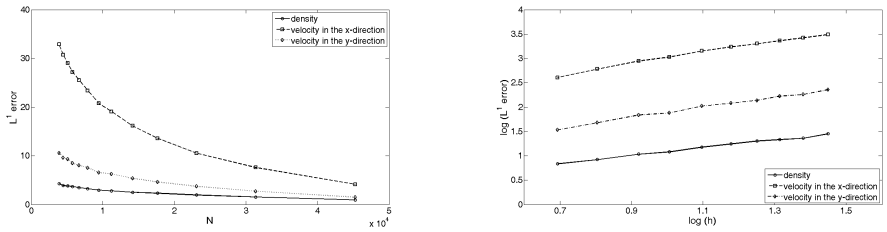

Figure 7: *Dependence of the L^1 errors of the density and the velocity in the x and y direction on the number of finite volume cells N (on the left) and the loglog plot of the errors with respect to the grid-spacing h (on the right)*

	Density	Velocity-x	Velocity-y
$T = 5$	0.8	1.14	1.05

Table 3: *Estimates of the order of the fully discrete scheme (18) for the second order model (1)*

data $\rho_0 = 1 \cdot \chi_{[1,5]\times[1,5]}\ ped/m^2$ and $\vec{v}_0 = 0\ m/s$ and parameters $v_{\max} = 2\ m/s$, $\rho_{\max} = 7\ ped/m^2$, $p_0 = 0.005$, $\gamma = 2$.

The L^1 error is computed using equation (33) with the reference mesh containing $N_{\text{ref}} = 70772$ finite volume cells. In Fig 7 we present the dependence at time $t = 5\ s$ of the L^1 error on the number of finite volume cells (on the left) and its loglog plot with respect to the grid-spacing parameter h_k. Table 3 shows the estimates of the convergence order of the scheme.

4.2 Comparison between the first and the second order models

Now we compare numerically the behaviour of Hughes model (4) and the second order model (1). We analyze the capability of the models of reproducing the formation of stop-and-go waves and we study the effect on the flow of obstacles placed in the proximity of an exit.

4.2.1 Stop and go waves

In high density crowd, pedestrians experience strong local interactions which can result in macroscopically observed phenomena. One of them, known from vehicular traffic flow, are stop-and-go waves, that is regions with high density and small speed which propagate backward. In the case of pedestrians such waves were observed in front of the entrance to the Jamarat Bridge on 12 January 2006 [21] and studied experimentally for a single lane [44, 34].

Simulating stop-and-go waves can be one of the criteria to validate a model, see for example [34] in case of microscopic description. In order to verify if macroscopic models are able to reproduce this phenomenon we consider a corridor $100m \times 20m$ with two, $1.2m$ wide exits centered symmetrically at $x = 67\ m$ and $x = 93\ m$, see Fig 8. The initial density is $\rho_0 = 3\chi_{[0,50]\times[6,26]}$ ped/m^2 and the initial velocity is set to zero. Fig 9 shows the density distribution at different times $t = 30, 40, 60\ s$ in four cases:

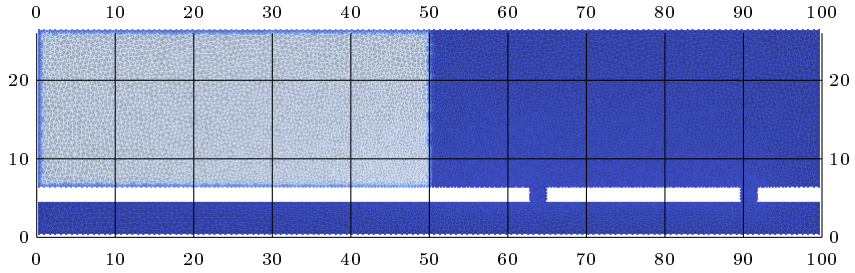

Figure 8: *A corridor* $100m \times 20m$ *with two,* 1.2 m *wide exits centered symmetrically at* $x = 67$ m *and* $x = 93$ m

Case I: the first order model (4) with the running cost function $c(\rho) = 1/v_{\max}$
Case II: the first order model (4) with the running cost function$c(\rho) = 1/V(\rho)$
Case III: the second order model (1) with $c(\rho) = 1/V(\rho)$ and $p_0 = 0.1$
Case IV: the second order model (1) with $c(\rho) = 1/V(\rho)$ and $p_0 = 0.005$

Other parameters are $v_{\max} = 2$ m/s, $\rho_{\max} = 10$ ped/m^2, $\gamma = 2$. We observe that in case (I) the alternative further exit is not used by pedestrians, who choose their route only on the basis of the shortest distance, not the shortest time, to the target. The distribution of density given by the first order model (I, II), apart from the proximity of the exit, is very smooth. A similar behaviour is obtained for the second order model with large pressure coefficient $p_0 = 0.1$ (III). High internal repealing forces between pedestrians prevent from congestion and formation of significant inhomogeneities in the density distribution. Decreasing p_0 allows for smaller distances between individuals, which causes stronger interactions. As a result for $p_0 = 0.005$ (IV) we observe sub-domains with much higher density. The locations of high density peaks are moving in the opposite direction to the flow. This propagation is clearly observed near the exit where characteristic arching appears. In Fig 10, we present a zoomed view of exits neighborhoods at different times. Stop-and-go waves start at the exits and move backwards. Fig 11 shows the density distribution profile along the y-direction originating at the center of one of the exits.

4.2.2 Bottlenecks

It was experimentally observed that flow of pedestrians through a bottleneck depends on its width (see for example [41, 32, 23]) and can be significantly slowed down due to clogging at its entrance. Blocking at bottlenecks occurs when the flow of pedestrians towards the door is much higher than the capacity of the exit. The density grows and, as a result, physical interactions between pedestrians increase, slowing down the motion and interrupting the outflow. From the point of view of evacuation strategies it is essential for a mathematical model to be able to capture this effect. We study numerically the behaviour of solutions of the first (4) and the second (1) order model during the evacuation through a narrow exit. We consider an empty room $10m \times 6m$ with a $1m$ wide, a symmetrically placed exit and different obstacles placed in its interior, see Fig 12,

obstacle 1: one column centered at $(8.5, 3)$ with radius $r = 0.3$ m
obstacle 2: three columns centered at $(9, 2.5), (8, 3), (9, 3.5)$ with radius $r = 0.2$ m
obstacle 3: two walls with $7.5 \leq x \leq 9$ and $2.3 \leq y \leq 2.5$, $3.5 \leq y \leq 3.7$

Fig 13 presents the time evolution of the total mass of pedestrians remaining inside the room for Hughes' model (4) (on the left) and for the second order model (1) (on the right) with $v_{\max} = 2$ m/s, $\rho_{\max} = 7$ ped/m^2, $P(\rho) = 0.005\rho^2$ and with initial data $\rho_0 = 1 \cdot \chi_{[1,5]\times[1,5]}$ ped/m^2. We observe that in the case of the first order model the total mass $M(t)$ decreases linearly and is the same for all obstacles and the empty room. The outflow is regulated only by the capacity of

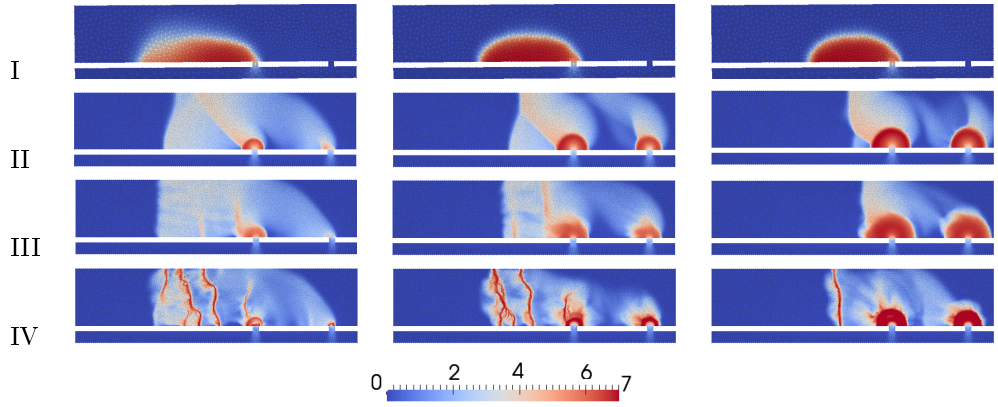

Figure 9: *Density profiles at different times t=30s (left), t=40s (middle), t=60s (right). I: First order model* (4) *with* $c(\rho) = 1/v_{\max}$ *(Simple model) II: First order model* (4) *with* $c(\rho) = 1/V(\rho)$ *(Hughes model) III: Second order model with* $c(\rho) = 1/V(\rho)$ *and* $p_0 = 0.1$ *IV: Second order model with* $c(\rho) = 1/V(\rho)$ *and* $p_0 = 0.005$*. Other parameters are* $v_{\max} = 2\ m/s$, $\rho_{\max} = 7\ ped/m^2$, $\gamma = 2$ *and initial data are* $\rho_0 = 3\chi_{[0,50]\times[6,26]}\ ped/m^2$ *and* $\vec{v}_0 = 0$.

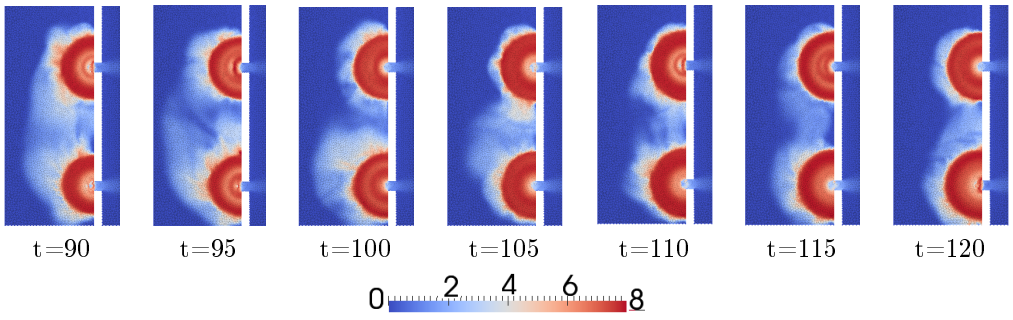

Figure 10: *Zoomed density profiles near the exits of the corridor* Ω^C *for the second order model* (1) *in the case* $P(\rho) = 0.005\rho^2$*. Other parameters are* $v_{\max} = 2\ m/s$, $\rho_{\max} = 7\ ped/m^2$, $\gamma = 2$ *and initial data are* $\rho_0 = 3\chi_{[0,50]\times[6,26]}\ ped/m^2$ *and* $\vec{v}_0 = 0$*. The figures are turned counterclockwise by 90 degrees.*

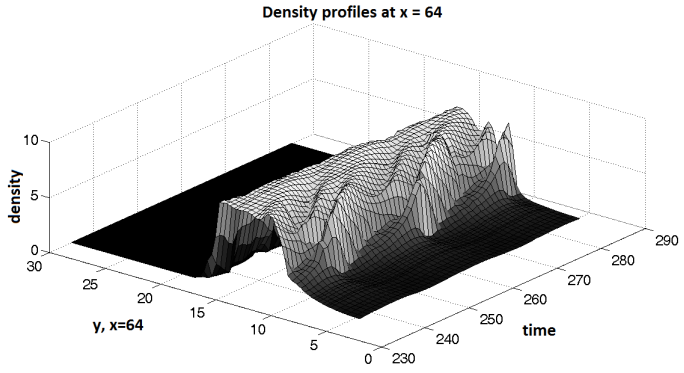

Figure 11: *Time evolution of a density profile along a line parallel to the y-axis and passing the center of the first exit* $(x, y) = (64, 6)$

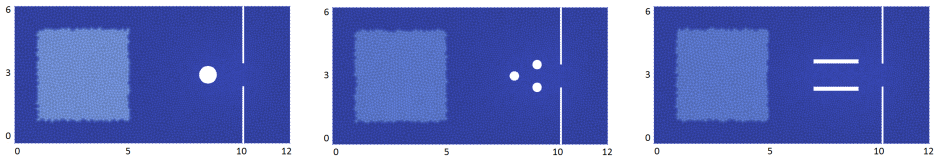

Figure 12: *A room of dimensions* $10m \times 6m$ *with a* $1m$ *wide, symmetrically placed exit and different obstacles placed in its interior. Obstacle 1: circle centered at* $(8.5, 3)$ *with radius* $r = 0.3$ m*. Obstacle 2: 3 circles centered at* $(9, 2.5), (8, 3), (9, 3.5)$ *with radius* $r = 0.2$ m*. Obstacle 3: 2 rectangles with* $7.5 \leq x \leq 9$ *and* $2.3 \leq y \leq 2.5$, $3.5 \leq y \leq 3.7$

the door. We do not observe either clogging, which would slow down the decrease of the total mass, or the influence of obstacles. The total evacuation time T_{evac} is basically the same for all situations. On the other hand, in the case of the second order model the empty room experiences a significant decrease of the outflow. It may correspond to clogging at the exit when a sufficiently large number of pedestrians reaches it. Obstacles play a role of a barrier and decrease the flow arriving at the exit. As a result, evacuation is slower but clogging is reduced. In Figs 14-17 we present the density profiles at different times for the Hughes model (4) (on top) and for the second order model (1) (on bottom).

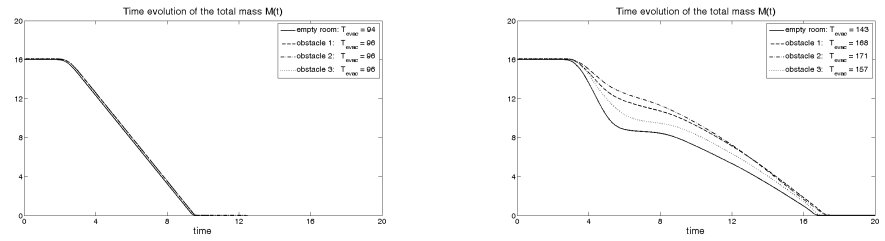

Hughes model Second order model

Figure 13: *Time evolution of the total mass $M(t)$ of pedestrians in the empty room and with three different obstacles. On the left: Hughes model* (4) *with* $v_{\max} = 2\ m/s$, $\rho_{\max} = 7\ ped/m^2$. *On the right: second order model* (1) *with* $v_{\max} = 2\ m/s$, $\rho_{\max} = 7\ ped/m^2$, $p_0 = 0.005$, $\gamma = 2$.

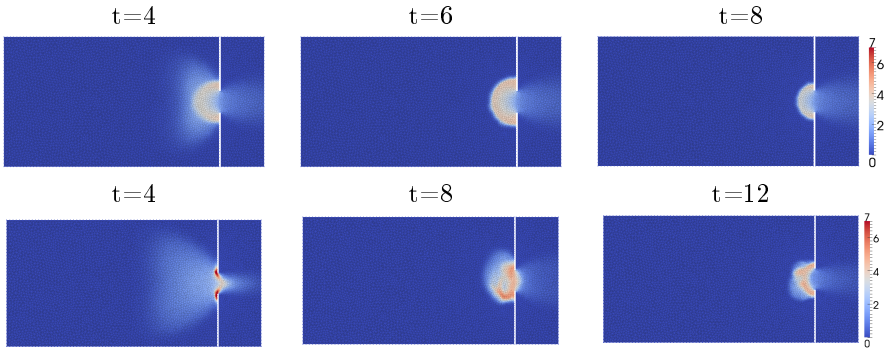

Figure 14: *Density profiles at different times for the Hughes model* (4) *(on top) and the second order model* (1) *(on bottom) with* $v_{\max} = 2\ m/s$, $\rho_{\max} = 7\ ped/m^2$, $p_0 = 0.005$, $\gamma = 2$, $M_0 = 16$.

4.3 Dependence on the parameters p_0, γ and $v_{\max}$

In the previous section we observed that the first order model (4) is unable to produce complex crowd behaviour such as stop-and-go waves and clogging at bottlenecks. This is why we now focus our analysis on the second order model (1) and explore the dependence of its solutions on the system parameters p_0, γ and $v_{\max}$. Our aim is to analyze how the degree of congestion of the crowd and the value of desired walking speed of pedestrians influence the evacuation time.

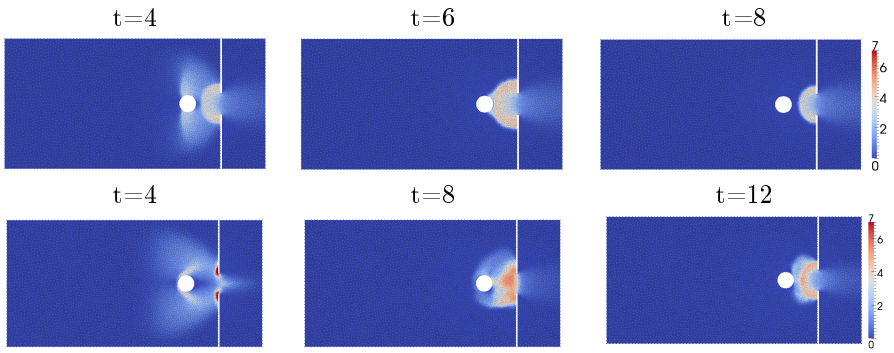

Figure 15: *Density profiles at different times for the Hughes model* (4) *(on top) and the second order model* (1) *(on bottom) with* $v_{\max} = 2\ m/s$, $\rho_{\max} = 7\ ped/m^2$, $p_0 = 0.005$, $\gamma = 2$, $M_0 = 16$.

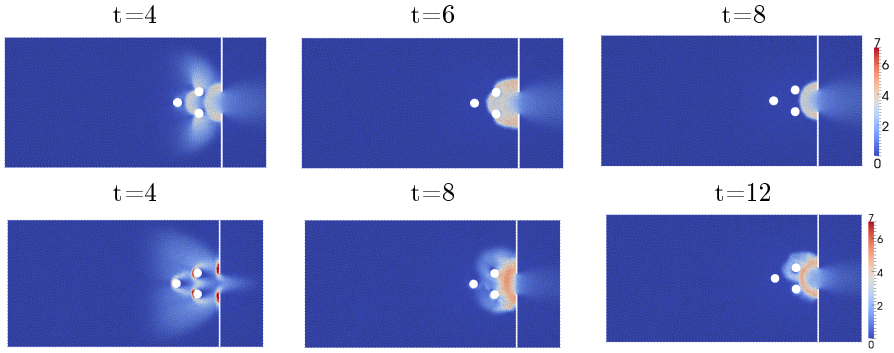

Figure 16: *Density profiles at different times for the Hughes model* (4) *(on top) and the second order model* (1) *(on bottom) with* $v_{\max} = 2\ m/s$, $\rho_{\max} = 7\ ped/m^2$, $p_0 = 0.005$, $\gamma = 2$, $M_0 = 16$.

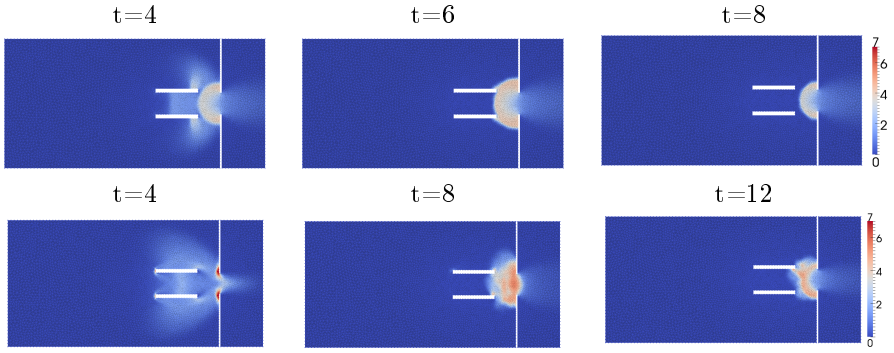

Figure 17: *Density profiles at different times for the Hughes model* (4) *(on top) and the second order model* (1) *(on bottom) with* $v_{\max} = 2\ m/s$, $\rho_{\max} = 7\ ped/m^2$, $p_0 = 0.005$, $\gamma = 2$, $M_0 = 16$.

4.3.1 Dependence on the parameters p_0 and γ

At first we analyze the dependence on the coefficients of the internal pressure function given by the law for isentropic gases (3). It describes the repealing forces between pedestrians and prevents from overcrowding. Under emergency and panic conditions the comfort zone of pedestrians, which defines how close they can stay to each other, decreases. As a result, the density of the crowd can increase and impedes the movement leading to discontinuous flow. As we have already seen, in Section (4.2.1), the formation of stop-and-go waves depend on the coefficient p_0. Now our aim is to study the relation between the strength of the repealing forces between pedestrians and the efficiency of the evacuation.

We consider an empty room $10m \times 6m$ with a 1 m wide, symmetrically placed exit and set the following initial data $\rho_0 = 1.5 \cdot \chi_{[1,5]\times[1,5]}\ ped/m^2$, $\vec{v}_0 = 0$. In Fig 18a we present the time evolution of the total mass of pedestrians remaining in the room for different values of the coefficient p_0 in the cases of adiabatic exponent $\gamma = 2$ and $v_{\max} = 2\ m/s$, $\rho_{\max} = 7\ ped/m^2$. We observe that for small values of p_0 there is a significant decrease of the outflow of pedestrians through the exit, which means that it is blocked. Increasing p_0 prevents from congestion and as a result the outflow is smother. However, when the distance between pedestrians increases, leaving the room becomes more time consuming. Fig 19 shows the dependence of the total evacuation time T_{evac} given by (31) on the parameter p_0 in the case of $\gamma = 2, 3$. We observe an optimal value of the parameter p_0, which minimizes the evacuation time of pedestrians from the room.

The effect of the adiabatic exponent γ is similar. High values increase the repealing forces between pedestrians. We present in Fig 20 the evolution of the total mass for $\gamma = 2, 3, 4, 5$. Clogging observed in the case $\gamma = 2$ diminishes for larger γ. For $\gamma = 5$ we observe quasi-linear decrease of the total mass.

The response of pedestrians to compression has an essential effect on the evacuation time. In normal conditions, when pedestrians want to keep a certain comfort and have enough free space to move, the outflow through the exit is undisturbed. During emergency situations the distances between individuals decrease and the density of the crowd increases, reducing the mobility of pedestrians. As a result the flow may become discontinuous and exits may be blocked. Our simulations show that the second order model is able to reproduce these phenomena.

4.3.2 Dependence on the desired speed $v_{\max}$

Now we look for the dependence of the total evacuation time on the desired speed $v_{\max}$ of pedestrians. Empirical studies indicate that the average free speed, that is the speed at which pedestrians walk when they are not influenced by others, is about 1.34 m/s with standard deviation of 0.37 m/s (see [6]). Due to impatience, emergency or panic, people tend to move faster to escape uncomfortable situation or direct life thread as soon as possible. Using the social force model [22] Helbing et al. [16] analyzed an evacuation of 200 people from a room for different desired speeds corresponding to different states of panic. Under the condition of high friction due to the tangential motion of pedestrians, they observed the existence of an optimal speed for which the evacuation was optimized. In Fig 22 we analyze the evacuation of pedestrians from the empty room $\Omega = [0, 10] \times [0, 6]m^2$ through a $1m$ wide exit with $\rho_0 = 2\chi_{[1,5]\times[1,5]}\ ped/m^2$, $\vec{v}_0 = 0$ for different values of the desired speed $v_{\max} = 0.5, 1.0, 1.5, 2.0, 3.0, 4.0, 6.0\ m/s$ in the case of $p_0 = 0.005$ (on the left) and $p_0 = 0.5$ (on the right).

We observe that unlike Helbing et al.[16], the total evacuation time decreases with higher desired speed, Fig 21. Pedestrians at the front of a group can move almost with at desired velocity $v_{\max}$ as they are not slowed down by the presence of others. When the free speed is high, they reach the exit very fast and leave the room in a short time. However, due to the limited flow capacity of the exit, in the case of $p_0 = 0.005$ we see that pedestrians start to accumulate in

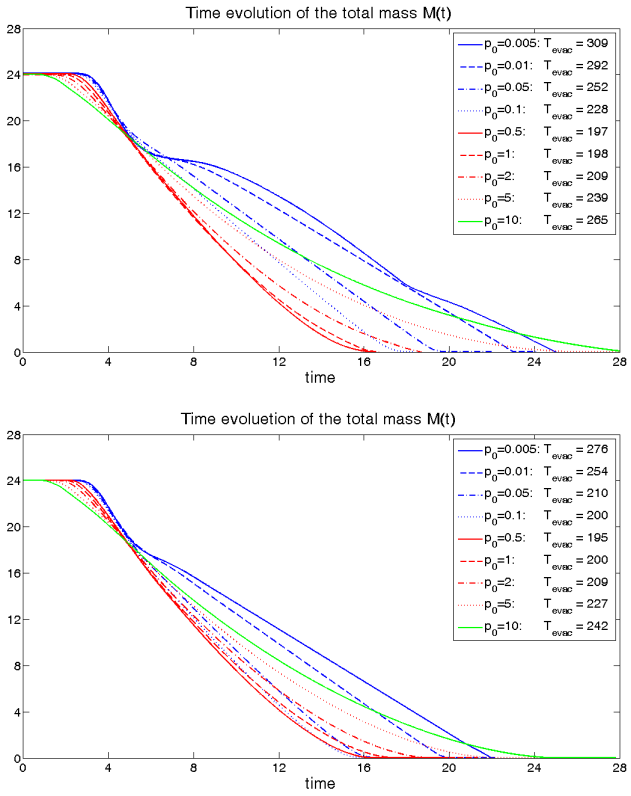

Figure 18: *Time evolution of the total mass $M(t)$ of pedestrians inside the room for the system* (1) *with* $v_{\max} = 2\ m/s$, $\rho_{\max} = 7\ ped/m^2$ *and* $\rho_0 = 1.5\chi_{[1,5]\times[1,5]}\ ped/m^2$, $\vec{v}_0 = 0$ *for different values of the pressure coefficient* $p_0 = 0.005, 0.01, 0.05, 0.1, 0.5, 1.0, 2.0, 5.0, 10.0$ *and for different values of the adiabatic exponent* $\gamma = 2$ *(on top) and* $\gamma = 3$ *(on bottom)*

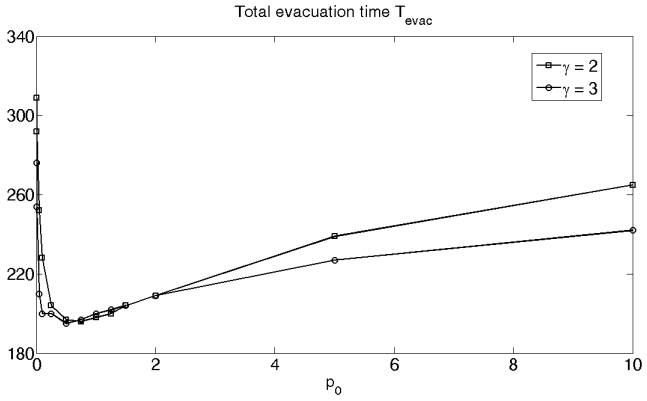

Figure 19: *Total evacuation time T_{evac} for the system* (1) *with* $v_{\max} = 2\ m/s$, $\rho_{\max} = 7\ ped/m^2$ *and* $\rho_0 = 1.5\chi_{[1,5]\times[1,5]}\ ped/m^2$, $\vec{v}_0 = 0$ *for different values of the pressure coefficient* $p_0 = 0.005, 0.01, 0.05, 0.1, 0.5, 1.0, 2.0, 5.0, 10.0$ *and for different adiabatic exponent* $\gamma = 2, 3$

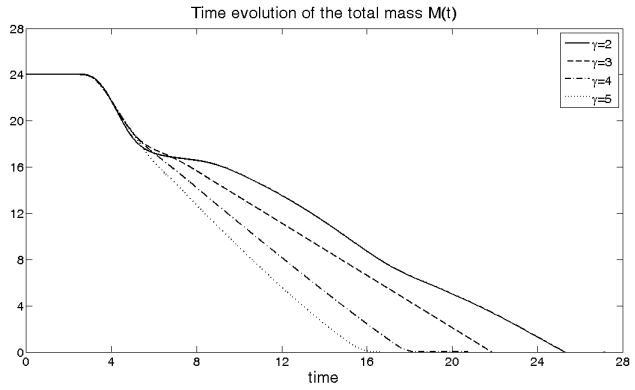

Figure 20: *Time evolution of the total mass of pedestrians inside the room* $M(t)$ *for the system* (1) *with* $v_{\max} = 2\ m/s$, $\rho_{\max} = 7\ ped/m^2$, $p_0 = 0.005$ *and* $\rho_0 = 1.5\chi_{[1,5]\times[1,5]}\ ped/m^2$, $\vec{v}_0 = 0$ *for different values the adiabatic exponent* $\gamma = 2, 3, 4, 5$.

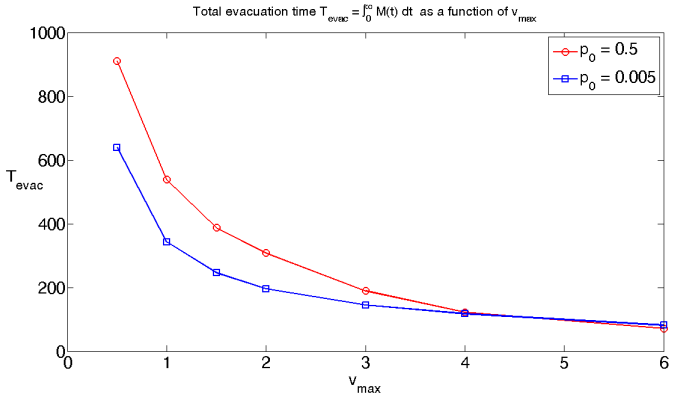

Figure 21: *Total evacuation time* T_{evac} *for the system* (1) *with* $\rho_{\max} = 7\ ped/m^2$, $\gamma = 2$, $\rho_0 = 1.5\chi_{[1,5]\times[1,5]}\ ped/m^2$, $\vec{v}_0 = 0$ *for different values of the desired velocity* $v_{\max} = 0.5, 1.0, 1.5, 2.0, 3.0, 4.0, 6.0$ *and for different pressure coefficients* $p_0 = 0.005$ *(on the left) and* $p_0 = 0.5$ *(on the right)*

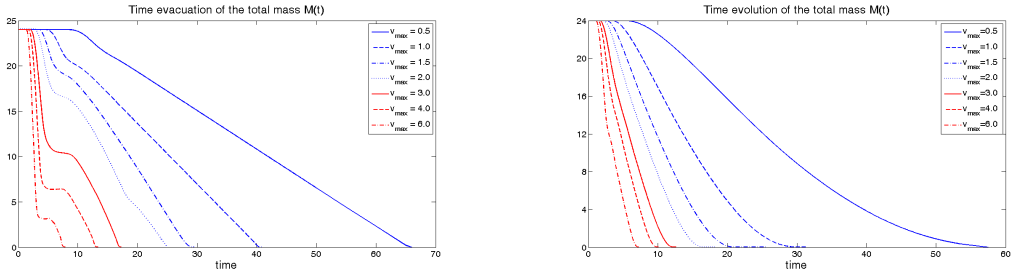

Figure 22: *Time evolution of the total mass of pedestrians inside the room $M(t)$ for the system* (1) *with $\rho_{\max} = 7$ ped/m^2, $\gamma = 2$ and $\rho_0 = 1.5\chi_{[1,5]\times[1,5]}$ ped/m^2, $\vec{v}_0 = 0$ for different values of the desired velocity $v_{\max} = 0.5, 1.0, 1.5, 2.0, 3.0, 4.0, 6.0$ m/s and for different pressure coefficients $p_0 = 0.005$ (on the left) and $p_0 = 0.5$ (on the right)*

front of the door and block it. Decreasing the value of $v_{\max}$ the flow through the exit decreases, so clogging occurs earlier than in the case of larger desired speed. At the same time, also the accumulation has a smaller rate, due to smaller $v_{\max}$, so the outflow is only slowed down instead of being blocked. Increasing the value of the internal pressure coefficient to $p_0 = 0.5$, the evacuation becomes faster and more regular compared to what we have already observed in the previous simulations. The difference in the results between the two models, macroscopic and microscopic, may be due to the lack of the sliding friction force impeding relative tangential motion in the macroscopic, second order model (1).

4.4 Effect of obstacles

In this section we study the evacuation from a room following the idea of Hughes [27], who raised the question of weather suitably placed obstacles can increase the flow through an exit. This idea is an inversion of the Braess paradox [3, 4], which was formulated for traffic flows and states that adding extra capacity to a network can in some cases reduce the overall performance. In the case of crowd dynamics, placing an obstacle may be seen intuitively as a worse condition. Nevertheless, it is expected to decrease the density in front of the exit and as a result prevent it from blocking.

This phenomenon has been studied experimentally in case of granular materials. More precisely, Zuriguel et al. [51] analyzed the outflow of grains from a silo and found out optimal hight above the outlet of an obstacle which reduces the blocking of the flow by a factor of one hundred. The authors indicated that clogging is caused by the spontaneous occurrence of arches over the outlet which have enough strength to hold up the rest of the granular material. A properly placed obstacle can decrease the pressure in the region of the arch formation and prevents the particles higher up in the container from weighting down on those in the vicinity of the outlet.

We examine closely this phenomenon in case of pedestrian motion using the second order model (1) with $v_{\max} = 2$ m/s, $\rho_{\max} = 7$ $peed/m^2$. In Section 4.2.2 we have already observed that an obstacle in front of an exit can reduce the clogging. In this section we consider a room $10m \times 6m$ with a 1 m wide, symmetrically placed exit and system of five circular columns arranged in the shape of a triangle opened towards the door. The columns are centered at $(9.5, 2), (9, 2.5), (8.5, 3), (9, 3.5), (9.5, 4)$ and have the radius $r = 0.22m$, see Fig 5 and the initial density equals $\rho_0 = 1$ ped/m^2 in the area $[1, 5]m \times [1, 5]m$.

In order to compare the efficiency of the evacuation we use the total mass of pedestrians

that remain in the room using (31), which corresponds directly to the outflow through the door. Fig 23 presents the time evolution of the total mass on meshes with different number of finite volume cells, which are refined by a factor two near the exit and the obstacles. The room with the columns and the obstacle-free case are considered. We observe that for the empty room (on top) the results do not change with the mesh refinement. On the contrary, in the case with the obstacles (on bottom) there is a significant difference between the total mass curves for $N = 16000, 26000$ and for $N = 6000, 8000$ finite volume cells. This effect is a result of the presence of phenomena occurring at different length scales for irregular flows. In Fig 24 we can see that the clogging observed on the mesh with $N = 16000$ finite volume cells is not resolved for $N = 6000$ resulting in false faster evacuation.

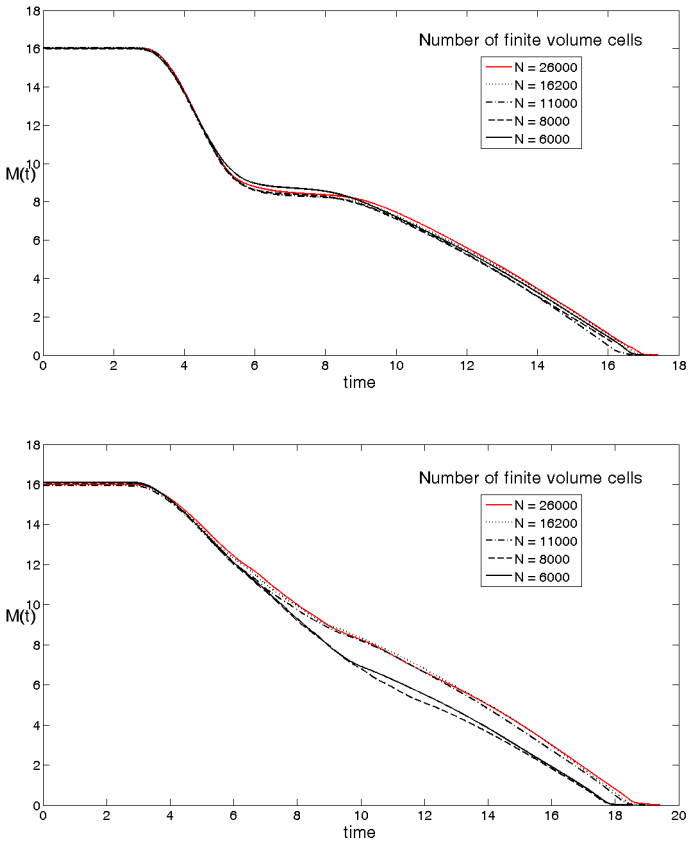

Figure 23: *Time evolution of the total mass of pedestrians $M(t)$ for the system* (1) *with $v_{\max} = 2\ m/s$, $\rho_{\max} = 7\ peed/m^2$, $p_0 = 0.005$, $\gamma = 2$ for different numbers of the finite volume cells in case of the empty room (on top) and with five columns in front of the exit (on bottom).*

In the following test we compare numerically the evacuation from the room described above using a mesh with $N = 16000$ finite volume cells. Fig 25 shows the time evolution of the total mass for two different pressure coefficients $p_0 = 0.005, 0.001$. We observe that the clogging present in the empty room is reduced significantly using the obstacles. The system of columns creates a "waiting zone" in front of the exit. Pedestrians are slowed down and partially stopped

by the obstacles, which corresponds to the slower outflow in the initial phase of the evacuation. But, at the same time the density at the exit remains low because the incoming flow doesn't exceed the door capacity. In case of small pressure $p_0 = 0.001$, which allows for higher congestion, the improvement due to the obstacles is more visible. For the initial mass $M = 32$ and columns of radius $r = 0.24\ m$ the total evacuation time of the room with the columns becomes smaller that in the obstacles-free situation.

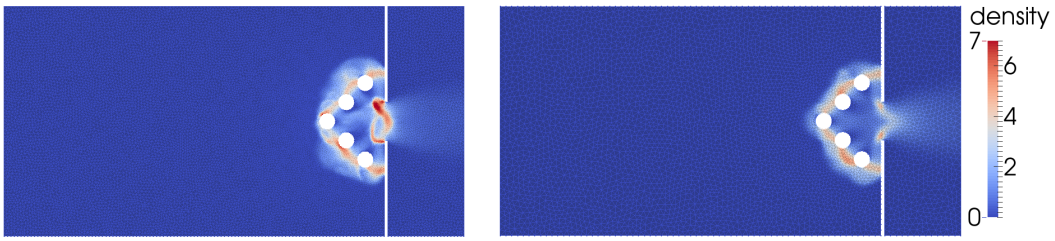

Figure 24: *Density profiles at time $T = 9$ of the system (1) with $v_{\max} = 2\ m/s$, $\rho_{\max} = 7\ peed/m^2$, $p_0 = 0.005$, $\gamma = 2$ for different numbers of the finite volume cells: $N = 16000$ (on the left) and $N = 6000$ (on the right).*

Acknowledgment

This research was supported by the ERC Starting Grant 2010 under the project "*TRAffic Management by Macroscopic Models*"

Contents

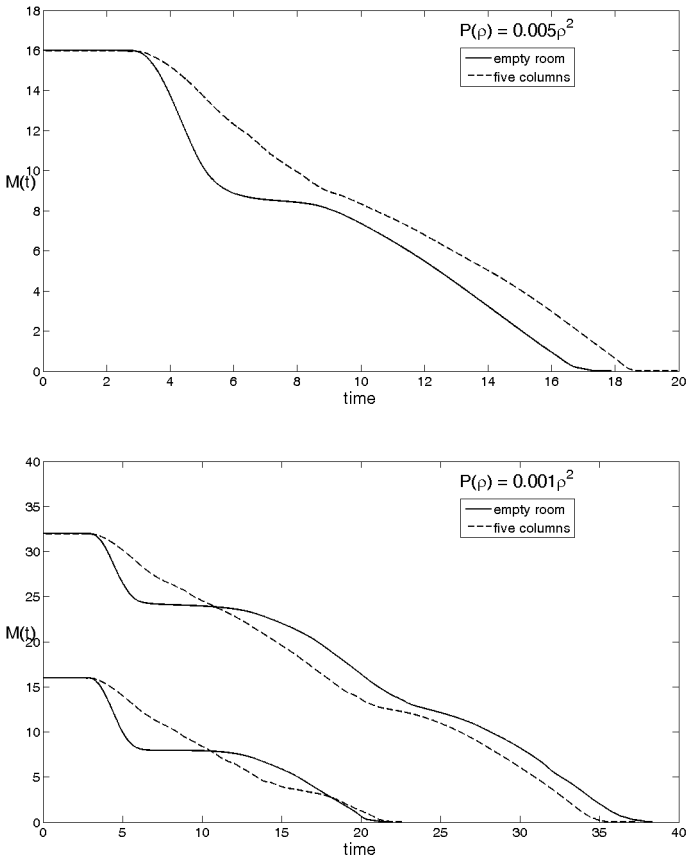

Figure 25: *Time evolution of the total mass of pedestrians* $M(t)$ *for the system* (1) *with* $v_{\max} = 2\ m/s$, $\rho_{\max} = 7\ peed/m^2$, $\gamma = 2$ *for different pressure coefficients:* $p_0 = 0.005$ *(on top) and* $p_0 = 0.001$ *(on bottom).*

References

[1] N. Bellomo and C. Dogbé. On the modelling crowd dynamics from scaling to hyperbolic macroscopic models, 2008.

[2] F. Bornemann and Ch. Rasch. Finite-element discretization of static Hamilton-Jacobi equations based on a local variational principle. *Comput. Vis. Sci.*, 9(2):57–69, 2006.

[3] D. Braess. Über ein Paradoxon aus der Verkehrsplanung. *Unternehmensforschung*, 12:258–268, 1968.

[4] D. Braess, A. Nagurney, and T. Wakolbinger. On a paradox of traffic planning. *Transportation Science*, 39(4):446–450, 2005.

[5] S. Bryson and D. Levy. High-order semi-discrete central-upwind schemes for multi-dimensional Hamilton-Jacobi equations. *J. Comput. Phys.*, 189(1):63–87, 2003.

[6] S. Buchmueller and U. Weidmann. *Parameters of Pedestrians, Pedestrian Traffic and Walking Facilities*. Schriftenreihe des IVT. Institute for Transport Planning and Systems (IVT), Chair of Transport Systems, ETH Zurich, 2006.

[7] R.M. Colombo and M.D. Rosini. Pedestrian flows and nonclassical shocks. 28(13):1553–1567, 2005.

[8] J. Dijkstra, H. J. P. Timmermans, and A. J. Jessurun. A multi-agent cellular automata system for visualising simulated pedestrian activity. In *in S. Bandini and T. Worsch (Eds.), Theoretical and Practical Issues on Cellular Automata - Proceedings on the 4th International Conference on Cellular Automata for research and Industry*, pages 29–36. Springer Verlag, 2000.

[9] B. Einfeldt, C. D. Munz, P. L. Roe, and B. Sjögreen. On Godunov-type methods near low densities. *J. Comput. Phys.*, 92(2):273–295, January 1991.

[10] R. Escobar and A. De La Rosa. Architectural design for the survival optimization of panicking fleeing victims. In Wolfgang Banzhaf, Thomas Christaller, Peter Dittrich, Jan T. Kim, and Jens Ziegler, editors, *Advances in Artificial Life, 7th European Conference, ECAL 2003, Dortmund, Germany, September 14-17, 2003, Proceedings*, volume 2801 of *Lecture Notes in Computer Science*, pages 97–106. Springer, 2003.

[11] M. Falcone and R. Ferretti. Semi-Lagrangian schemes for Hamilton-Jacobi equations, discrete representation formulae and Godunov methods. *J. Comput. Phys.*, 175(2):559–575, 2002.

[12] G.A. Frank and C.O. Dorso. Room evacuation in the presence of an obstacle. *Physica A: Statistical Mechanics and its Applications*, 390(11):2135–2145, 2011.

[13] S. Gopal and T. R. Smith. Navigator: an ai-based model of human way-finding in an urban environment. *Spatial Choices and Processes, eds. M.M. Fischer, P. Nijkamp and Y.Y. Papageorgiou (North-Holland Elsevier Science Publishers)*, pages 169–200.

[14] A. Harten, P. D. Lax, and B. van Leer. On Upstream Differencing and Godunov-Type Schemes for Hyperbolic Conservation Laws. *Siam Review*, 25, 1983.

[15] D. Helbing, L. Buzna, A. Johansson, and Torsten Werner. Self-organized pedestrian crowd dynamics: Experiments, simulations, and design solutions. *Transportation Science*, 39(1):1–24, 2005.

[16] D. Helbing, I. Farkas, P. Molnàr, and T. Vicsek. Simulation of pedestrian crowds in normal and evacuation situations. In M. Schreckenberg and S. D. Sharma, editors, *Pedestrian and Evacuation Dynamics*, pages 21–58, Berlin, 2002. Springer.

[17] D. Helbing, I. Farkas, and T. Vicsek. Simulating Dynamical Features of Escape Panic. *Nature*, 407:487–490, September 2000.

[18] D. Helbing, I. Farkas, and T. Vicsek. Crowd disasters and simulation of panic situations. In *The Science of Disasters*, pages 330–350. Springer Berlin Heidelberg, 2002.

[19] D. Helbing, I.J. Farkas, and T. Vicsek. Freezing by heating in a driven mesoscopic system. *Phys. Rev. Lett.*, 84:1240–1243, Feb 2000.

[20] D. Helbing and A. Johansson. Pedestrian, crowd and evacuation dynamics. In Robert A. Meyers, editor, *Encyclopedia of Complexity and Systems Science*, pages 6476–6495. Springer, 2009.

[21] D. Helbing, A. Johansson, and H. Zein Al-Abideen. Dynamics of crowd disasters: An empirical study. *Physical Review E (Statistical, Nonlinear, and Soft Matter Physics)*, 75(4):046109, 2007.

[22] D. Helbing and P. Molnàr. Social force model for pedestrian dynamics. *Physical Review E*, pages 4282–4286, 1995.

[23] S.P. Hoogendoorn and W. Daamen. Pedestrian behavior at bottlenecks. *Transportation Science*, 39(2):147–159, 2005.

[24] Ch. Hu and Ch.W. Shu. A discontinuous Galerkin finite element method for Hamilton-Jacobi equations. *SIAM J. Sci. Comput.*, 21(2):666–690 (electronic), 1999.

[25] L. Huang, S.C. Wong, M. Zhang, C.-W. Shu, and W.H.K. Lam. Revisiting hughes' dynamic continuum model for pedestrian flow and the development of an efficient solution algorithm. *Transportation Research Part B: Methodological*, 43(1):127–141, 2009.

[26] R. L. Hughes. A continuum theory for the flow of pedestrians. *Transportation Research Part B: Methodological*, 36(6):507 – 535, 2002.

[27] R.L. Hughes. The flow of human crowds. In *Annual review of fluid mechanics, Vol. 35*, volume 35 of *Annu. Rev. Fluid Mech.*, pages 169–182. Annual Reviews, Palo Alto, CA, 2003.

[28] Inria. Num3sis software, 2012.

[29] Y.-Q Jiang, R.-X. Liu, and Y.-L. Duan. Numerical simulation of pedestrian flow past a circular obstruction. *Acta Mech. Sin.*, 27(2):215–221, 2011.

[30] Y.Q. Jiang, P. Zhang, S.C. Wong, and R.X. Liu. A higher-order macroscopic model for pedestrian flows. *Physica A: Statistical Mechanics and its Applications*, 389(21):4623 – 4635, 2010.

[31] J. P. Keating. The myth of panic. *Fire Journal*, May:57–62, 1982.

[32] T. Kretz, A. Grünebohm, and M. Schreckenberg. Experimental study of pedestrian flow through a bottleneck. *Journal of Statistical Mechanics: Theory and Experiment*, 2006(10):P10014, 2006.

[33] J. Labroquère, R. Duvigneau, T. Kliczko, and J. Wintz. Interactive computation and visualization towards a virtual wind tunnel. *in 47th 3AF Symposium on Applied Aerodynamics, Paris, France,*, March, 2012.

[34] S. Lemercier, A. Jelic, R. Kulpa, J. Hua, J. Fehrenbach, P. Degond, C. Appert-Rolland, S. Donikian, and J. Pettré. Realistic following behaviors for crowd simulation. *Comp. Graph. Forum*, 31(2pt2):489–498, May 2012.

[35] B. Maury, A. Roudneff-Chupin, and F. Santambrogio. A macroscopic crowd motion model of gradient flow type, 2009.

[36] M. Muramatsu, T. Irie, and T. Nagatani. Jamming transition in pedestrian counter flow. *Physica A: Statistical and Theoretical Physics*, 267(3-4):487–498, May 1999.

[37] S. Osher and R. Fedkiw. *Level set methods and dynamic implicit surfaces*, volume 153 of *Applied Mathematical Sciences*. Springer-Verlag, New York, 2003.

[38] S. Osher and J. A. Sethian. Fronts propagating with curvature-dependent speed: algorithms based on Hamilton-Jacobi formulations. *J. Comput. Phys.*, 79(1):12–49, 1988.

[39] H.J. Payne. *Models of Freeway Traffic and Control*. Simulation Councils, Incorporated, 1971.

[40] B. Piccoli and A. Tosin. Pedestrian flows in bounded domains with obstacles. *Contin. Mech. Thermodyn*, 21(2):85–107, 2009.

[41] V.M. Predtechenskii and A.I. Milinskii. *Planning for Foot Traffic Flow in Buildings*. TT. Amerind, 1978.

[42] P. J. Roache. Perspective: A Method for Uniform Reporting of Grid Refinement Studies. *Journal of Fluids Engineering*, 116(3):405–413, 1994.

[43] J. A. Sethian. *Level set methods and fast marching methods*, volume 3 of *Cambridge Monographs on Applied and Computational Mathematics*. Cambridge University Press, Cambridge, second edition, 1999. Evolving interfaces in computational geometry, fluid mechanics, computer vision, and materials science.

[44] A. Seyfried, M. Boltes, J. KÃ¤hler, W. Klingsch, A. Portz, T. Rupprecht, A. Schadschneider, B. Steffen, and A. Winkens. Enhanced empirical data for the fundamental diagram and the flow through bottlenecks. In *Pedestrian and Evacuation Dynamics 2008, / ed.: W.W.F. Klingsch, C.Rogsch, A. Schadschneider, M.Schreckenberg, Berlin/Heidelberg, Springer, 2010. - 978-3-642-04503-5. - S. 145 - 156*, 2010. Record converted from VDB: 12.11.2012.

[45] A. Seyfried, O. Passon, B. Steffen, M. Boltes, T. Rupprecht, and W. Klingsch. New insights into pedestrian flow through bottlenecks. *Transportation Science*, 43(3):395–406, 2009.

[46] A. Seyfried, B. Steffen, and T. Lippert. Basics of modelling the pedestrian flow. *Physica A*, 368:232–238, 2006.

[47] E.F. Toro. *Riemann Solvers and Numerical Methods for Fluid Dynamics: A Practical Introduction*. Springer-Verlag Berlin Heidelberg, 2009.

[48] Y. R. Tsai, L.-T. Cheng, S. Osher, and H.K. Zhao. Fast sweeping algorithms for a class of Hamilton-Jacobi equations. *SIAM J. Numer. Anal.*, 41(2):673–694, 2003.

[49] G.B. Whitham. *Linear and nonlinear waves*. Pure and applied mathematics. Wiley, 1974.

[50] Y. Xia, S. C. Wong, and Ch.W. Shu. Dynamic continuum pedestrian flow model with memory effect. *Phys. Rev. E*, 79:066113, Jun 2009.

[51] I. Zuriguel, A. Janda, A. Garcimart'in, C. Lozano, R. Arévalo, and D. Maza. Silo Clogging Reduction by the Presence of an Obstacle. *Physical Review Letters*, 107:278001+, December 2011.

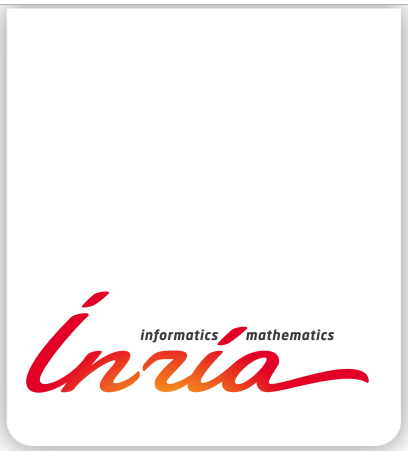

RESEARCH CENTRE
SOPHIA ANTIPOLIS – MÉDITERRANÉE

2004 route des Lucioles - BP 93
06902 Sophia Antipolis Cedex

Publisher
Inria
Domaine de Voluceau - Rocquencourt
BP 105 - 78153 Le Chesnay Cedex
inria.fr

ISSN 0249-6399